Biallelic variants in *SLC35B2* cause a novel chondrodysplasia with hypomyelinating leukodystrophy

Alessandra Guasto,[1] Johanne Dubail,[1,†] Sergio Aguilera-Albesa,[2,3,†] Chiara Paganini,[4] Catherine Vanhulle,[5] Walid Haouari,[6] Nerea Gorría-Redondo,[2] Elena Aznal-Sainz,[3] Nathalie Boddaert,[7] Laura Planas-Serra,[8,9] Agatha Schlüter,[8,9] Edgard Verdura,[8,9] Arnaud Bruneel,[6,10] Antonio Rossi,[4] Céline Huber,[1] Aurora Pujol[8,9,11] and Valérie Cormier-Daire[1,12]

1 Paris Cité University, INSERM UMR1163, Imagine Institute, 75015 Paris, France

2 Pediatric Neurology Unit, Department of Pediatrics, Complejo Hospitalario de Navarra, Navarrabiomed, Pamplona, Spain

3 Children's Medically Complex Diseases Unit, Department of Pediatrics, Complejo Hospitalario de Navarra, Pamplona, Spain

4 Department of Molecular Medicine, Unit of Biochemistry, University of Pavia, Pavia, Italy

5 Service de Neuropédiatrie, pavillon Martainville, Hôpital Charles Nicolle, 76031, Rouen, France

6 INSERM UMR1193, Paris-Saclay University, F-92220 Châtenay-Malabry, France

7 Service d'Imagerie pédiatrique, AP-HP, Hôpital Necker-Enfants malades, F-75015 Paris, France

8 Neurometabolic Diseases Laboratory, Bellvitge Biomedical Research Institute (IDIBELL), L'Hospitalet de Llobregat, 08908, Barcelona, Catalonia, Spain

9 Centre for Biomedical Research in Network on Rare Diseases (CIBERER), Instituto de Salud Carlos III, 28029, Madrid, Spain

10 AP-HP, Biochimie métabolique et cellulaire, Hôpital Bichat, F-75018, Paris, France

11 Catalan Institution of Research and Advanced Studies (ICREA), Barcelona, Catalonia, Spain

12 Service de Génétique clinique, Centre de référence pour les maladies osseuses constitutionnelles, AP-HP, Hôpital Necker-Enfants malades, F-75015 Paris, France

Correspondence to: Valérie Cormier-Daire

Clinical Genetics, Necker Enfants Malades hospital, INSERM UMR1163, Imagine Institute, 24 Boulevard du Montparnasse 75015 Paris, France

E-mail: valerie.cormier-daire@inserm.fr

Correspondence may also be addressed to: Aurora Pujol

Bellvitge Biomedical Research Institute (IDIBELL), L'Hospitalet de Llobregat, 08908, Barcelona, Catalonia, Spain

E-mail: apujol@idibell.cat

†**These authors contributed equally to this work.**

Running title: Role of *SLC35B2* in bone and brain disease

Abstract

Sulfated proteoglycans are essential in skeletal and brain development. Recently, pathogenic variants in genes encoding proteins involved in the proteoglycan biosynthesis have been identified in a range of chondrodysplasia associated with intellectual disability. Nevertheless, several patients remain with unidentified molecular basis. This study aimed to contribute to the deciphering of new molecular bases in patients with chondrodysplasia and neuro-developmental disease.

Exome sequencing was performed to identify pathogenic variants in patients presenting with chondrodysplasia and intellectual disability. The pathogenic effects of the potentially causative variants were analyzed by functional studies.

We identified homozygous variants (c.1218_1220del and c.1224_1225del) in *SLC35B2* in two patients with pre- and postnatal growth retardation, scoliosis, severe motor and intellectual disabilities and hypomyelinating leukodystrophy. By functional analyses, we showed that the variants affect *SLC35B2* mRNA expression and protein subcellular localization leading to a functional impairment of the protein. Consistent with those results, we detected proteoglycan sulfation impairment in *SLC35B2* patient fibroblasts and serum.

Our data support that SLC35B2 functional impairment causes a novel syndromic chondrodysplasia with hypomyelinating leukodystrophy, most likely through a proteoglycan sulfation defect. This is the first time that *SLC35B2* variants are associated with bone and brain development in human.

Keywords: SLC35B2; chondrodysplasia; hypomyelinating leukodystrophy; proteoglycans

Introduction

Proteoglycans (PGs) are organic macromolecules abundantly modified by sulfation through the addition of sulfate to their covalently attached GAG chains by membrane-bound sulfotransferases located in the Golgi apparatus. The major source of intracellular sulfate pool comes from the extracellular environment thanks to a specific sulfate/chloride antiporter of the plasma membrane.[1] In the cytosol, this sulfate is then activated to the universal sulfate donor 3'-phosphoadenosine 5'-phosphosulfate (PAPS) by PAPS synthases. Because most of the sulfation of glycoconjugates occurs in the Golgi apparatus, PAPS is translocated by PAPS transporters (PAPST1 and PAPST2 also named SLC35B2 and SLC35B3) from the cytoplasm into the Golgi lumen where it serves as substrate for the sulfotransferases.[2]

Sulfated PGs can be present on the cell surface or in the ECM. They play a role in many fundamental processes, in embryonic development, as co-receptors for growth factors and in regulation of cell growth and differentiation.[3,4] Thanks to their macromolecular structure and negative charge, they have significant roles in the maintenance of mechanical proprieties of cartilage, in the lubrication of joints, and in the stabilization of collagen fibers.[5–7] In addition, PGs are essential for brain development since they participate in proliferation and differentiation of neural progenitors, maturation and plasticity of synapses, migration and axon pathfinding, myelination and axon regeneration.[8]

Since PGs are major components of connective tissue, defects in PG biosynthesis lead to skeletal and connective tissue disorders and may also cause intellectual and psychiatric disorders.

Recently, pathogenic variants in genes encoding proteins involved in PG biosynthesis have been identified in a group of chondrodysplasia.[9] More specifically, the identification of several pathogenic variants in genes involved in different steps of PG sulfation, leading to GAG

sulfation defects, have supported the importance of adequate PG sulfation level in bone development.[10]

Within this group of rare disorders, several patients present a combination of chondrodysplasia and intellectual disability and a few of them remain with unknown molecular basis.

In this study, using exome sequencing (ES), we identified homozygous variants in *SLC35B2* in two patients presenting with a chondrodysplasia, a severe intellectual disability and hypomyelinating leukodystrophy. *SLC35B2* encodes a member of the solute carrier family located in the Golgi apparatus membrane. It transports the activated nucleotide sulfate PAPS from cytosol, where it is synthetized, into the Golgi lumen, where the PG sulfation occurs. Using *in vitro* functional studies, we demonstrate that functional impairment of SLC35B2 disrupts GAG sulfation in patient fibroblasts and serum.

Materials and Methods

Family recruitment and sampling

The first affected individual (patient 1 from family A) was included in a research project for undiagnosed chondrodysplasia with multiple dislocations, characterized by severe pre- and post-natal growth retardation, large joint dislocations, and scoliosis. The second patient (patient 2 from family B) was included in a research project for undiagnosed leukodystrophies at IDIBELL Institute. Venous blood was obtained for DNA extraction from affected and control individuals (QIAamp DNA blood Maxi kit, QIAGEN). Fibroblast cultures were established from skin biopsies obtained from scalp incision.

Informed consent for participation and sample collection were obtained via protocols approved by the Necker Hospital Ethics Board Committee and by the Clinical Research Ethics Committees of IDIBELL Institute (PR076/14), respectively.

Whole exome sequencing

Genomic DNA was extracted from leucocytes. Variants were filtered using the URD-Cat platform (https://rdcat.cnag.crg.eu/, with a frequency lower than 0.01 in the ExAC, 1000 Genomes and gnomAD databases, and deleterious effect was evaluated using several predictors (PolyPhen-2, SIFT, CADD, and Mutation Taster). Further information about this method is included in Supplementary material.

Sanger sequencing analysis of *SLC35B2*

Exon 4 of *SLC35B2* was amplified with specific primers (Supplementary Table 1). Amplification products were purified by ExoSapIT (Amersham) and directly sequenced with the Big Dye Terminator Cycle Sequencing Ready Reaction kit v1.1 on an automatic sequencer (3500XL; PE Applied Biosystems). Sequence analyses were performed with the analysis software, Sequencing 6 (Applied Biosystems) and Gensearch (PhenoSystems SA).

Q-PCR

Analysis of *SLC35B2*, *GAPDH* and *RPLP0* gene expression levels was performed with a ViiA 7 Real-Time PCR system (Applied Biosystems) using the fast SYBR™ green master mix (Applied Biosystems) and specific primers (Supplementary Table 1). Each sample was run in triplicate in 96 well plates in three independent experiments. The levels of the *SLC35B2* transcript were normalized to those of *GAPDH* or *RPLP0* and reported as a fold of change. The comparative CT method was used in this study.

SLC35B2 expression plasmids

Control skin primary fibroblasts were cultured in RPMI medium supplemented with 10% fetal calf serum. Total RNAs from fibroblast monolayers were extracted using the Rneasy Mini kit (Qiagen) according to the manufacturer's instructions. *SLC35B2* cDNA was amplified after reverse transcription of RNA using the specific primers (Supplementary Table 1). The resulting amplicon was cloned into pcDNA™3.1/Myc-His A + (Invitrogen) to generate proteins with an in-frame Myc-His Tag and then sequenced to verify the correct insertion. The mutant construct for the first patient (patient 1 from family A) was then generated using a Q5® Site-Directed Mutagenesis kit (New England Biolabs) and two mutagenic primers (Supplementary Table 1). The mutant construct for the second patient (patient 2 from family B) was generated by two sequential reactions using a Q5® Site-Directed Mutagenesis kit (New England Biolabs) and four mutagenic primers (Supplementary Table 1). The presence of the variants was verified by Sanger sequencing.

Recombinant protein expression

HEK293F cells were cultured in DMEM supplemented with 10% fetal bovine serum (FBS). Transfections were performed on cells in 12-well plates or in 8-chamber labtek slides (ThermoFisher Scientific) using jet-PRIME® transfection reagent (Polyplus Transfection) according to the manufacturer's instructions. For western blotting, cells in 12-well plates were collected 72 h after transfection and lysed in denaturation buffer. Polyacrylamide gel electrophoresis, transfer and immunoblotting were performed according to standard protocols using monoclonal anti-myc (9E10; 1/1000; Santa Cruz Biotechnologies) or monoclonal anti-actin (clone C4; 1/5000; Millipore) primary antibodies and goat anti-mouse HRP-conjugated secondary antibody (1/1000; Novex, Life Technologies). For immunofluorescence, cells in 8-

chamber slides were fixed 48 h after transfection with 4% paraformaldehyde (PFA) at RT for 30 min. The washed cell layer was incubated sequentially in phosphate-buffered saline (PBS) containing 1% bovine serum albumin (BSA) for 30 min, mouse monoclonal anti-GM130 (clone 35, 1/200; BD Biosciences) for 1 h, polyclonal anti-myc (9E10, Alexa –Fluor 555 conjugate; 1/100; Millipore) for 1h and Alexa Fluor 594 goat anti-mouse IgG (1/200; Life Technologies) for 1 h. After mounting in Prolong gold antifade mountant with DAPI (Molecular Probes, Life Technologies) cells were observed with an Axioplan2 imaging microscope (Zeiss).

HPLC analysis of chondroitin sulfate disaccharides in cultured fibroblasts

For chondroitin sulfate (CS) sulfation dosage, we used fibroblasts established from 2 patient and 5 control skin biopsies. Controls have been selected according to patient age and gender. Fibroblast were incubated with or without 1 mM of 4-nitrophenyl β-D-xylopyranoside (β-xyloside, Sigma-Aldrich) in DMEM without FBS at 37°C in 5% CO_2 for 24 h. Medium were then collected and incubated overnight at 65°C with 2.5 U/ml of papain (Sigma) in digestion buffer at a final concentration of 0.1 M sodium acetate, pH 5.6, 5 mM EDTA and 5 mM cysteine. Samples were incubated at 100°C for 10 min to inactivate papain and released GAGs were precipitated overnight at RT with 1% (w/v) cetylpyridinium chloride (final concentration). The samples were centrifuged at 13000 x g for 15 min. The pellets were washed three times with 10% potassium acetate in 96% ethanol, three times with 96% ethanol and then air dried. The precipitates were solubilized in 0.1 M ammonium acetate pH 7.35 and digested overnight at 37°C with 20 mU chondroitinase ABC (AMSBIO) and 20 mU chondroitinase ACII (Sigma-Aldrich) in a final volume of 200 µl. Samples were then cleared by centrifugation at 13000 x g for 15 min, and the supernatants were lyophilized. The lyophilizates were dissolved in 40 µl of

12.5 mM 2-aminoacridone (Life Technologies) in 85:15 (v/v) dimethyl sulfoxide:glacial acetic acid and incubated in the dark for 15 min before adding 40 µl of 1.25 M $NaBH_3CN$ (Sigma-Aldrich). Then samples were incubated at 37°C overnight in the dark. GAG samples were analysed by an HPLC system (1525µ Binary HPLC Pump, Waters). Chromatography was carried out as previously reported.[11] The elution profile was measured with a fluorescent detector (2475 Multi λ Fluorescence Detector, Waters) set at λ_{ex} 425 nm and λ_{em} 525 nm.

Bikunin electrophoretic profiles

For analysis of serum bikunin, blood samples were collected in tubes without any anticoagulant to allow clot formation. Sera were obtained after centrifugation for 15 min at 2000 x g. Classical SDS-PAGE was carried out as previously described[12] using 4–12% NuPAGE Bis-Tris gels. Two-dimensional gel electrophoresis (2-DE) was carried out on serum treated by chondroitinase ABC, as previously described using ZOOM Strip pH 4–7 for the first dimension and 4–12% NuPAGE Bis-Tris gels for the second dimension[12]. In both cases, after transfer on nitrocellulose, ECL revelation was conducted after incubation with rabbit anti-bikunin primary antibodies (1/5000; Merck-Millipore) and secondary HRP-linked anti-rabbit antibodies (1/5000; Cell Signaling technologies). Images were acquired using a Chemidoc XRS camera system from Bio-Rad.

Statistics

Statistical analyses were performed using GraphPad PRISM. All values are shown as mean ± SD. Statistical differences between two groups were analyzed with a two-tailed Student's t-test, assuming a normal distribution. A *p*-value of < 0.05 was considered statistically significant.

Data availability

More detailed data are provided in the online supplementary file. The data that support the findings of this study are available on request from the corresponding authors.

Results

Phenotype of *SLC35B2* patients

Patient 1

The first patient (patient 1 from family A) is the third child of healthy first cousin parents from Moroccan origin. During pregnancy, polyhydramnios and short femora (< 3rd percentiles) were detected at 22 weeks of gestation. Ultrasound survey revealed short long bones contrasting with normal head circumference (HC), supporting a diagnosis of chondrodysplasia but no specific diagnosis was made. She was born at 38 weeks of gestation. At birth, her weight was 3275 g (M), height 42 cm (-4 SD) and HC 36 cm. She presented with adducted thumbs, dislocations of elbows, knee and ulna deviation. A cleft palate was also detected with retrognathia and glossoptosis leading to a diagnosis of Pierre Robin sequence. She had feeding difficulties in the first months of life and psychomotor delay. At 5 months of age, she had no head control and major hyperlaxity. Skeleton X rays revealed short long bones, hip and elbow dislocations (Figure 1A, B), advanced carpal ossification (Figure 1B), and hypoplastic cervical vertebrae (C3-C4). She benefited from physiotherapy and speech therapy. She had surgery for cleft palate at 18 months of age. At 32 months of age, her weight was 8450 g, height 66 cm (< -6 SD), and HC 50.5 cm (-0.5 SD). Brain magnetic resonance imaging (MRI) revealed hypomyelinating leukodystrophy, i.e. an abnormal development of the white matter of the brain, corpus callosum

hypoplasia and cerebral atrophy (Figure 2 A-F). At 12 years of age, she had no speech, no walk and no spontaneous mobility but flessum of elbows and knees, valgus deformities of feet, lumbar scoliosis (Figure 1C), requiring seat brace, and facial dysmorphism including flat face and retrognathia. She had surgery for right hip dislocation (Figure 1D). Her growth parameters were height 88 cm (< -8 SD) and weight < -5 SD.

Patient 2

The second patient (patient 2 from family B) is the first child of healthy unrelated parents from Spanish origin. Oligohydramnios and intrauterine growth restriction (< p10) was detected at week 37 of gestation. Patient was born at 38 weeks of gestation after a cesarean delivery. Birth weight was 1634 g (< -3 SD), length was 41.5 cm (< -4 SD) and HC was 30.5 cm (< -3 SD). At 2 months of age, axial hypotonia with scoliosis was noticed. Cerebral MRI revealed an infra and supratentorial complete absence of myelination (Figure 2G-I). From 3 months of age, a horizontal nystagmus was detected. At 6 months of age, control MRI showed no progression of myelination in supra and infratentorial structures. MR spectroscopy did not reveal any white matter abnormal peaks. At that age, axial hypotonia was severe. At 24 months, her growth parameters were height < -3 SD, weight < -3 SD and HC < -2 SD. At 36 months, axial hypotonia was moderate to severe and eye-hand coordination activities were limited. Horizontal nystagmus persisted. At that age, cerebral MRI still showed no progression of myelination, with thin corpus callosum (Figure 2 J-L). At 8 years of age, her growth parameters were height < -4 SD and weight < -2 SD. She was able to keep standing with mild support and perform a few side steps with aid. Axial hypotonia was moderate, with no signs of spasticity. Mild limb dystonia was noticed. She was able to communicate with single words and hand signs. Remarkably, nerve conduction studies showed no significant abnormalities. Skeleton X rays revealed a thoracic

scoliosis, but also hip anomalies with *coxa valga* and insufficient acetabular coverage, small epiphyses around the knees and abnormal epiphyseal ulna (Figure 1E-H). Brain MRI at 8 years of age showed no progression of myelination, with thin corpus callosum and mild cerebral and cerebellar atrophy (Figure 2M-O).

Identification of homozygous *SLC35B2* variants by exome sequencing in two patients with chondrodysplasia and hypomyelinating leukodystrophy

Exome sequencing (ES) in patient 1 (from family A) revealed a homozygous missense variant in *CUL7* gene (c.3184C>T, p.Arg1062Trp), responsible for 3 M syndrome (OMIM 273750) characterized by facial features, pre-and postnatal growth retardation (< – 3SD) and slender long bones. However, the severity of the short stature (< – 8SD), the presence of major skeletal features (scoliosis, dislocations of large joints, advanced carpal ossification, Pierre Robin sequence) and intellectual disability, never observed in 3 M syndrome, prompted us to study further the ES data. This study led to the identification of an in frame deletion in the exon 4 (c.1218_1220del, p.Leu407del) of *SLC35B2* (NM_178148.3, Figure 3A). The *SLC35B2* deletion affected a leucine residue at codon 407, a highly conserved amino acid in the predicted protein transporter domain (Figure 3B). The *SLC35B2* variant has never been reported in dbSNP, EXAC, GnomAD and public databases. This variant was confirmed by Sanger sequencing, present at the homozygous state in the patient and at the heterozygous state in her unaffected parents and sisters (Figure 3C). Sharing this variant through GeneMatcher[13], we identified a similarly affected patient with a biallelic variant in the same gene. ES performed in patient 2 (from family B) identified a homozygous deletion in the exon 4 of the *SLC35B2* gene (c.1224_1225delAG, p.Arg408SerfsTer18) (Figure 3A). This frameshift deletion causes the loss of an arginine at codon 408, giving rise to a premature stop codon after 17 amino acids and a truncated protein lacking the

last 8 amino acids (Figure 3B). This variant, which is absent from dbSNP, EXAC, GnomAD and other public databases, was present at the homozygous state in the patient and was heterozygous in her unaffected mother, while absent from father. Thorough analysis of ES data revealed a chromosome 6 uniparental isodisomy (iUPD) in the patient, spanning the complete chromosome 6 (Figure 3C). No other variants of interest were detected in the case.

The *SLC35B2* gene contains 4 exons and is mapped on chromosome 6p21.1. This gene encodes a member of the solute carrier family SLC35. The deduced 432-amino acid protein has a calculated molecular mass of 47.5 kDa and eight transmembrane domains. SLC35B2 mediates the transport of PAPS from the cytosol into the Golgi lumen. Thus, due to its transporter function, SLC35B2 is involved in the sulfation of PG GAG chains. *SLC35B2* high mRNA expression has been reported in placenta, pancreas, skeletal muscle, cerebellum, mammary glands, as well as in endocrine tissues, proximal digestive tract and gastrointestinal tract, and in fetal and adult mouse brain including neural/oligodendroglial progenitor niches in hippocampus and dentate gyrus [14,15] https://www.proteinatlas.org/ENSG00000157593-SLC35B2/tissue) (Supplementary Figure 1A). We thus investigated mRNA expression in human brain samples by qPCR analysis and found good expression of *SLC35B2* across the brain, most prominent in frontal lobe grey matter, subcortical frontal white matter, and cerebellum (Supplementary Figure 1B). Moreover, mouse brain single-cell RNA data available at the EMBL-EBI Single Cell Expression Atlas show a high expression of *Slc35b2* mRNA in oligodendrocytes and microglial cells (Supplementary Figure 1C).

SLC35B2 variants impact mRNA expression and causes protein mislocalization in transfected HEK293F cells

By RT-PCR analysis performed on mRNA extracted from skin fibroblasts, we measured a significant decrease of *SLC35B2* mRNA level in both patient fibroblasts compared to controls

(Figure 4A). Because of the absence of commercially available specific antibodies against the SLC35B2 protein, we decided to further analyze the functional consequences of *SLC35B2* variants using C-terminal c-myc tagged wild-type and mutant SLC35B2 proteins in parallel transfections of HEK293F cells. C-myc tagged protein expression was analyzed 72h after transfection. By western blotting on cell lysates, we did not detect any significant difference in the expression levels of the SLC35B2 mutant protein compared to the wild-type one (Figure 4B). We then studied the subcellular expression of mutant and wild-type SLC35B2 proteins. By c-myc immunolabelling, we showed that wild-type SLC35B2 colocalized with GM130, a specific marker for the Golgi apparatus, demonstrating that the wild-type protein is specifically expressed in the Golgi apparatus, as previously described.[15] However, for the mutant SLC35B2 constructs, a diffuse c-myc staining with only partial colocalization with GM130 was seen, suggesting a loss of localization specificity (Figure 4C). Together, these results demonstrate a similar deleterious impact of the two identified variants on *SLC35B2* gene expression and SLC35B2 protein subcellular localization.

Chondroitin sulfate disaccharide sulfation is altered in *SLC35B2* patient fibroblasts

Based on the known function of SLC35B2 in PG biosynthesis, we further studied the GAG sulfation pattern in fibroblast cultures from the patients and appropriate controls. Since CS chains are more abundant than the heparan sulfate (HS), we focused on the CS disaccharide sulfation profile. In addition, because PGs are not abundantly produced in fibroblasts in basal conditions, we increased GAG synthesis by addition to the culture medium of p-nitrophenyl-β-D-xylopyranoside (β-D-xyloside), a compound acting as a chain initiator. CS were extracted from the culture medium of cells incubated in basal condition and in presence of β-D-xyloside

and, after digestion with chondroitinases ABC and ACII, released disaccharides were derivatized with AMAC and analyzed by reverse-phase HPLC. In basal conditions, we detected a slight increase of the non-sulfated disaccharides of CS (ΔDi-0S) associated with a decrease of the monosulfated disaccharides of CS (ΔDi-4S and ΔDi-6S) in the patients compared to controls. These differences were significant when the fibroblasts were treated with β-D-xyloside: the percentage of ΔDi-0S was 11.3% and 6.5% in patient 1 and 2, respectively, vs 1.4% ± 0.3 in controls (n = 5) (*p*-value ≤0.01) (Figure 5A).

Abnormal bikunin electrophoretic pattern in *SLC35B2* patient serum

To further confirm the PG sulfation impairment, we looked at bikunin (Bkn) in patient and control sera. Bkn is a PG of liver origin that circulates in the blood under various forms including the free core Bkn protein and the form bearing a single CS chain (Bkn-CS). As shown in Figure 5B, western blot applied to controls (C1 to C4) and patient 1 (Pt) sera differentiated the core Bkn protein (~24 kDa) and the heterogeneous Bkn-CS form (34-37 kDa), without significant qualitative or quantitative abnormalities for the patient.

Since Bkn-CS form is heavily sulfated and thus highly acidic, it cannot be separated using 2-DE. Thus, as schematized Figure 5C, sera were treated by chondroitinase ABC in order to generate high amounts of a hexasaccharide-linked Bkn form (Bkn-Hex) carrying a reduced number of sulfation sites. Under these conditions, 2-DE patterns of controls either showed one (C1) or two spots (C2) with the more acidic one (‘left spot’) being highly predominant. For patients, 2 spots were distinguishable with a marked increased staining of the ‘right spot’ (arrow) compared to controls, demonstrating a loss of negative charges consistent with CS hyposulfation (Figure 5D).

Discussion

We report here the identification of homozygous variants in the *SLC35B2* gene in two patients with chondrodysplasia and severe hypomyelinating leukodystrophy. The skeletal phenotype is characterized by pre- and postnatal growth retardation and early scoliosis in both patients, dislocations of large joints and Pierre Robin sequence in one of them. Of particular importance, the patients present a severe psychomotor delay, predominantly in motor and expressive language development, and a hypomyelinating leukodystrophy with thin corpus callosum. Such severe neurological features have not been previously reported in the group of chondrodysplasias caused by PG biosynthesis defect and expand their phenotypic spectrum, constituting a novel, recognizable syndromic entity, also widening the growing landscape of metabolic genes associated with myelin formation and development.[16–18]

Since the identified variants were both localized in the last transmembrane domain (TMD) of SLC35B2 protein, we expected to have a similar impact on the protein structure and function.

Our results showed decreased expression level of *SLC35B2* mRNA in both patient fibroblasts and, although protein expression levels detected by western blot in transfected HEK293F cells were normal, our functional studies further support that the variants are responsible for a functional impairment of SLC35B2. Indeed, by immunofluorescence assay, we confirm the Golgi membrane localization of the wild-type protein contrasting with the partial mislocalization of the mutated proteins with diffuse signal in the cell. Several evidences show that TMDs are determinant for the membrane protein subcellular localization to the Golgi apparatus.[19, 20] Moreover, bioinformatics analysis of membrane proteins showed a strong correlation between the intracellular localization of the proteins and the exact amino acid composition of their TMDs and that a single amino acid substitution can cause the loss of protein localization specificity.[21, 22] These evidences may explain

why the two identified variants located in the last SLC35B2 TMD are responsible for the loss of the protein Golgi membrane localization. Our findings of decreased CS sulfation, both by HPLC disaccharide analysis and bikunin 2-DE western blot, further supported the functional impairment consequences of SLC35B2 variants, suggesting that the protein mislocalization from the Golgi results in decreased PAPS transport into the Golgi and consequently decreased GAG sulfation.

In the past years, several genetic defects have been linked to variants affecting different steps of PG sulfation and leading to a huge number of diseases that primarily affect cartilage and bone.[10] So far, no human genetic disorders have been linked to variants in *SLC35B2* gene, but cartilage defects have been reported in *slc35b2* null zebrafish mutant (pinscher, pic/slc35b2). Decreased level of total sulfated GAGs has been observed in pic zebrafish characterized by severe cartilage and bone defects.[23] It is intriguing that the *SLC35B2* patients reported in this study also showed a severe intellectual disability and brain structural anomalies, with hypomyelinating leukodystrophy, thin corpus callosum, cerebral and cerebellar atrophy. Several variants in genes implicated in PG biosynthesis are responsible not only for skeletal and connective tissue disorders but also for intellectual and psychiatric disorders. These include, for example, pathogenic variants in the xylosyltransferase-1 (*XYLT1*)[24] and the galactosyltransferase II *(B3GALT6)*[25] in the common linker region synthesis, causing connective tissue disease and intellectual disability; pathogenic variant in the chondroitin synthase 1 (*CHSY1*) causing skeletal anomalies and delayed motor and neural development;[26] and finally pathogenic variants in dermatan 4-O-sulfotransferase 1 (*CHST14*) causing Ehlers-Danlos syndrome with cranial ventricular enlargement and psychomotor retardation.[27]

The link between PG synthesis impairment and intellectual disorders might be due to the role of sulfated PGs in several processes during brain development. Sulfate conjugation is an essential

step during fetal brain development. Sulfation of HSPGs is important in neurogenesis, and CSPGs modulate neural cell guidance and neuronal outgrowth in the developing fetal brain.[28] Moreover, the higher expression of *SLC35B2* in fetal brain compared to adult brain confirms the importance of sulfation in the first steps of development.[15] Previous studies have supported a role of SLC35B2 in neuronal development. Indeed, the C-elegans model lacking *pst-1*, the nematode ortholog of human *SLC35B2,* showed that this protein is required for specific defects in the migration, axonal guidance, fasciculation and presynaptic development in a restricted subset of neurons. Moreover, this report showed that neuronal defects correlate with reduced complexity of HS modification patterns suggesting that pst-1 is important to establish the complex HS modification patterns that are required for neuronal connectivity.[29] Another study performed in Xenopus oocytes expressing *dsm-1* (D-serine-modulator-1), the rat ortholog of *SLC35B2*, confirms a pivotal role in the brain.[30] *Dsm-1* mRNA is predominantly expressed in the rat brain and in particular in the D-serine and NMDA receptor-rich brain regions suggesting a role of *dsm-1* in the regulation of D-serine metabolism. In Xenopus oocytes, the expression of dsm-1 accelerates the efflux of D-serine, the endogenous co-agonist for the NMDA receptor. Indeed, dysfunctions in the interactions of D-serine-NMDA receptors are involved in the pathophysiology of neuropsychiatric disorders and of spinocerebellar degeneration.[31,32] Of note, D-serine inhibits the first step and rate-limiting enzyme of the *de novo* sphingolipid synthesis, the serine palmytoyltransferase SPTLC1.[33] Loss of SPTLC1 activity leads to sensory neuropathy[34] and two steps further in the pathway, loss of the sphingolipid desaturase DEGS1 causes a severe hypomyelinating leukodystrophy with similar MRI presentation to the patients described here.[35] Indeed, PAPS are also sulfate donor for sulfation of glycolipids, such as galactosylceramide. In the Golgi, galactosylceramide reacts with PAPS to make sulfatide.[36]

Sulfatide is a pivotal component of the myelin sheath. Its deficiency leads to myelin malfunction,[37] while accumulation of sulfatides causes metachromatic leukodystrophy.[16]

Interestingly, pathogenic variants in other members of the SLC superfamily have already been associated with brain-bone phenotype. For example, SLC17A5 is involved in sialic acid storage diseases characterized by short stature, long bone metaphysis and hip dysplasia, clubbed feet, mental retardation and hypomyelination of the basal ganglia;[38] SLC35A3 is involved in congenital disorders of N-linked glycosylation (CDG) characterized by limb deformities, knee and hip dislocations, arthrogryposis, epilepsy and mild mental retardation;[39] SLC29A3 is involved in dysosteosclerosis characterized by sclerosis and increased bone fragility, short stature and epilepsy. Finally, variants in SLC35A2, have been associated with a rare X-linked form of CDG characterized by abnormal facial and skeletal features as shortened extremities, scoliosis and hip dislocations, epilepsy, psychomotor developmental delay, intellectual disability, spasticity and with a mild malformation of cortical development with oligodendroglial hyperplasia in epilepsy (MOGHE).[40,41]

We conclude that loss-of-function biallelic variants in *SLC35B2* are responsible for a severe autosomal recessive form of chondrodysplasia with hypomyelinating leukodystrophy. Our study demonstrates, for the first time, a link between *SLC35B2* and the development and function of bone and brain in humans.

Acknowledgements

We are grateful to the families for providing samples and the Asociación Española contra las Leucodistrofias (ALE-ELA España) for help and support. We are indebted to the National Institutes of Health NIH NeuroBioBank for supplying the case material used for human studies. We are indebted to Juan José Martinez at IDIBELL for technical support. We thank the Genomic

and the Bioinformatic facilities of Imagine Institute and the CNAG in Barcelona, Spain, for help in exome sequencing analysis. We thank GeneMatcher, a web-based tool for linking investigators with an interest in the same gene: https://genematcher.org/statistics/.

Funding

This work was supported by the Agence Nationale de la Recherche [ANR-18-CE14-0040 SKELGAG, to VCD] funding, by the Fondation pour la Recherche Médicale (FRM – "FDT202012010388", to AG) and MIUR [Dipartimenti di Eccellenza 2018–2022, to AR). Work at IDIBELL was supported by the PERIS program URD-Cat SLT002/16/00174), the Autonomous Government of Catalonia (SGR 2017SGR1206) and the Center for Biomedical Research on Rare Diseases (CIBERER) (ACCI19-759) to A.P. This study was also funded by Fundació La Marató de TV3 (595/C/2020), the Hesperia Foundation, the Ministerio de Ciencia e Innovación y Universidades (Juan de la Cierva, FJCI-2016-28811 to E.V.). We thank the CERCA Program/Generalitat de Catalunya for institutional support.

Competing interests

The authors report no competing interests.

Supplementary material

Supplementary material is available at Brain online.

References

1. Hästbacka J, de la Chapelle A, Mahtani MM, et al. The diastrophic dysplasia gene encodes a novel sulfate transporter: Positional cloning by fine-structure linkage disequilibrium mapping. *Cell*. 1994;78(6):1073-1087. doi:10.1016/0092-8674(94)90281-X

2. Ishida N, Kawakita M. Molecular physiology and pathology of the nucleotide sugar transporter family (SLC35). *Pfl*[?]*gers Archiv European Journal of Physiology*. 2004;447(5):768-775. doi:10.1007/s00424-003-1093-0

3. Karamanos NK, Theocharis AD, Neill T, Iozzo RV. Matrix modeling and remodeling: A biological interplay regulating tissue homeostasis and diseases. *Matrix Biol*. 2019;75-76:1-11. doi:10.1016/j.matbio.2018.08.007

4. Theocharis AD, Karamanos NK. Proteoglycans remodeling in cancer: Underlying molecular mechanisms. *Matrix Biol*. 2019;75-76:220-259. doi:10.1016/j.matbio.2017.10.008

5. Funderburgh JL. MINI REVIEW Keratan sulfate: structure, biosynthesis, and function. *Glycobiology*. 2000;10(10):951-958. doi:10.1093/glycob/10.10.951

6. Rabenstein DL. Heparin and heparan sulfate: structure and function. *Nat Prod Rep*. 2002;19(3):312-331. doi:10.1039/b100916h

7. Sugahara K. Recent advances in the structural biology of chondroitin sulfate and dermatan sulfate. *Current Opinion in Structural Biology*. 2003;13(5):612-620. doi:10.1016/j.sbi.2003.09.011

8. Schwartz NB, Domowicz MS. Proteoglycans in brain development and pathogenesis. *FEBS Lett*. 2018;592(23):3791-3805. doi:10.1002/1873-3468.13026

9. Dubail J, Cormier-Daire V. Chondrodysplasias With Multiple Dislocations Caused by Defects in Glycosaminoglycan Synthesis. *Front Genet*. 2021;12:642097. doi:10.3389/fgene.2021.642097

10. Paganini C, Gramegna Tota C, Superti-Furga A, Rossi A. Skeletal Dysplasias Caused by Sulfation Defects. *IJMS*. 2020;21(8):2710. doi:10.3390/ijms21082710

11. Paganini C, Monti L, Costantini R, et al. Calcium activated nucleotidase 1 (CANT1) is critical for glycosaminoglycan biosynthesis in cartilage and endochondral ossification. *Matrix Biology*. 2019;81:70-90. doi:10.1016/j.matbio.2018.11.002

12. Haouari W, Dubail J, Lounis-Ouaras S, et al. Serum bikunin isoforms in congenital disorders of glycosylation and linkeropathies. *Jrnl of Inher Metab Disea*. Published online August 7, 2020:jimd.12291. doi:10.1002/jimd.12291

13. Sobreira N, Schiettecatte F, Valle D, Hamosh A. GeneMatcher: a matching tool for connecting investigators with an interest in the same gene. *Hum Mutat*. 2015;36(10):928-930. doi:10.1002/humu.22844

14. Dahlin A, Royall J, Hohmann JG, Wang J. Expression profiling of the solute carrier gene family in the mouse brain. *J Pharmacol Exp Ther*. 2009;329(2):558-570. doi:10.1124/jpet.108.149831

15. Kamiyama S, Suda T, Ueda R, et al. Molecular Cloning and Identification of 3'-Phosphoadenosine 5'-Phosphosulfate Transporter. *J Biol Chem*. 2003;278(28):25958-25963. doi:10.1074/jbc.M302439200

16. Pant DC, Aguilera-Albesa S, Pujol A. Ceramide signalling in inherited and multifactorial brain metabolic diseases. *Neurobiol Dis*. 2020;143:105014. doi:10.1016/j.nbd.2020.105014

17. Dunn TM, Tifft CJ, Proia RL. A perilous path: the inborn errors of sphingolipid metabolism. *J Lipid Res*. 2019;60(3):475-483. doi:10.1194/jlr.S091827

18. Wolf NI, Ffrench-Constant C, van der Knaap MS. Hypomyelinating leukodystrophies - unravelling myelin biology. *Nat Rev Neurol*. 2021;17(2):88-103. doi:10.1038/s41582-020-00432-1

19. Kikegawa T, Yamaguchi T, Nambu R, Etchuya K, Ikeda M, Mukai Y. Signal-anchor sequences are an essential factor for the Golgi-plasma membrane localization of type II membrane proteins. *Bioscience, Biotechnology, and Biochemistry*. 2018;82(10):1708-1714. doi:10.1080/09168451.2018.1484272

20. Swift AM, Machamer CE. A Golgi retention signal in a membrane-spanning domain of coronavirus E1 protein. *Journal of Cell Biology*. 1991;115(1):19-30. doi:10.1083/jcb.115.1.19

21. Cosson P, Perrin J, Bonifacino JS. Anchors aweigh: protein localization and transport mediated by transmembrane domains. *Trends in Cell Biology*. 2013;23(10):511-517. doi:10.1016/j.tcb.2013.05.005

22. Land MA, Chapman HL, Davis-Reyes BD, et al. Serotonin 5-HT2C Receptor Cys23Ser Single Nucleotide Polymorphism Associates with Receptor Function and Localization In Vitro. *Sci Rep*. 2019;9(1):16737. doi:10.1038/s41598-019-53124-2

23. Wiweger MI, Avramut CM, de Andrea CE, et al. Cartilage ultrastructure in proteoglycan-deficient zebrafish mutants brings to light new candidate genes for human skeletal disorders: Zebrafish model for skeletal disorders. *J Pathol*. 2011;223(4):531-542. doi:10.1002/path.2824

24. Schreml J, Durmaz B, Cogulu O, et al. The missing "link": an autosomal recessive short stature syndrome caused by a hypofunctional XYLT1 mutation. *Hum Genet*. 2014;133(1):29-39. doi:10.1007/s00439-013-1351-y

25. Malfait F, Kariminejad A, Van Damme T, et al. Defective Initiation of Glycosaminoglycan Synthesis due to B3GALT6 Mutations Causes a Pleiotropic Ehlers-Danlos-Syndrome-like Connective Tissue Disorder. *The American Journal of Human Genetics*. 2013;92(6):935-945. doi:10.1016/j.ajhg.2013.04.016

26. Li Y, Laue K, Temtamy S, et al. Temtamy Preaxial Brachydactyly Syndrome Is Caused by Loss-of-Function Mutations in Chondroitin Synthase 1, a Potential Target of BMP Signaling. *The American Journal of Human Genetics*. 2010;87(6):757-767. doi:10.1016/j.ajhg.2010.10.003

27. Dündar M, Müller T, Zhang Q, et al. Loss of Dermatan-4-Sulfotransferase 1 Function Results in Adducted Thumb-Clubfoot Syndrome. *The American Journal of Human Genetics*. 2009;85(6):873-882. doi:10.1016/j.ajhg.2009.11.010

28. Dawson PA. Sulfate in fetal development. *Seminars in Cell & Developmental Biology*. 2011;22(6):653-659. doi:10.1016/j.semcdb.2011.03.004

29. Bhattacharya R, Townley RA, Berry KL, Bülow HE. The PAPS transporter PST-1 is required for heparan sulfation and is essential for viability and neural development in *C. elegans*. *J Cell Sci*. 2009;122(24):4492-4504. doi:10.1242/jcs.050732

30. Shimazu D, Yamamoto N, Umino A, Ishii S, Sakurai S ichiro, Nishikawa T. Inhibition of d-serine accumulation in the Xenopus oocyte by expression of the rat ortholog of human 3'-phosphoadenosine 5'-phosphosulfate transporter gene isolated from the neocortex as d-serine modulator-1. *J Neurochem*. 2006;96(1):30-42. doi:10.1111/j.1471-4159.2005.03501.x

31. Kumashiro S, Hashimoto A, Nishikawa T. Free d-serine in post-mortem brains and spinal cords of individuals with and without neuropsychiatric diseases. *Brain Research*. 1995;681(1-2):117-125. doi:10.1016/0006-8993(95)00307-C

32. Ogawa M, Shigeto H, Yamamoto T, et al. d-Cycloserine for the treatment of ataxia in spinocerebellar degeneration. *Journal of the Neurological Sciences*. 2003;210(1-2):53-56. doi:10.1016/S0022-510X(03)00009-1

33. Hanada K, Hara T, Nishijima M. D-Serine inhibits serine palmitoyltransferase, the enzyme catalyzing the initial step of sphingolipid biosynthesis. *FEBS Lett*. 2000;474(1):63-65. doi:10.1016/s0014-5793(00)01579-9

34. Bejaoui K, Uchida Y, Yasuda S, et al. Hereditary sensory neuropathy type 1 mutations confer dominant negative effects on serine palmitoyltransferase, critical for sphingolipid synthesis. *J Clin Invest*. 2002;110(9):1301-1308. doi:10.1172/JCI16450

35. Pant DC, Dorboz I, Schluter A, et al. Loss of the sphingolipid desaturase DEGS1 causes hypomyelinating leukodystrophy. *J Clin Invest*. 2019;129(3):1240-1256. doi:10.1172/JCI123959

36. Eckhardt M. The role and metabolism of sulfatide in the nervous system. *Mol Neurobiol*. 2008;37(2-3):93-103. doi:10.1007/s12035-008-8022-3

37. Honke K. Biosynthesis and biological function of sulfoglycolipids. *Proc Jpn Acad Ser B Phys Biol Sci*. 2013;89(4):129-138. doi:10.2183/pjab.89.129

38. Adams D, Wasserstein M. Free Sialic Acid Storage Disorders. In: Adam MP, Ardinger HH, Pagon RA, et al., eds. *GeneReviews®*. University of Washington, Seattle; 1993. Accessed February 21, 2022. http://www.ncbi.nlm.nih.gov/books/NBK1470/

39. Paprocka J, Jezela-Stanek A, Tylki-Szymańska A, Grunewald S. Congenital Disorders of Glycosylation from a Neurological Perspective. *Brain Sci*. 2021;11(1):88. doi:10.3390/brainsci11010088

40. Ng BG, Buckingham KJ, Raymond K, et al. Mosaicism of the UDP-galactose transporter SLC35A2 causes a congenital disorder of glycosylation. *Am J Hum Genet*. 2013;92(4):632-636. doi:10.1016/j.ajhg.2013.03.012

41. Miyamoto S, Nakashima M, Ohashi T, et al. A case of de novo splice site variant in SLC35A2 showing developmental delays, spastic paraplegia, and delayed myelination. *Mol Genet Genomic Med*. 2019;7(8):e814. doi:10.1002/mgg3.814

Figure legends

Figure 1: Skeletal features of *SLC35B2* patients. A, B) Patient 1 (from family A) X-rays at 5 months of age showing short long bones and hip dislocations (**A,** red arrow), advanced carpal ossification (**B**, red arrow indicating the presence of 3 ossification centers instead of one), dislocation of elbows (**B**, blue arrow) and ulna deviation (**B,** green arrow). **C, D**) Patient 1 (from family A) X-rays at 12 years of age showing lumbar scoliosis (**C**, red arrow) and hip with nailing surgery for right hip dislocation (**D**, red arrow).

E, H) Patient 2 (from family B) X-rays at 8 years of age showing mild flattening of the epiphyses around the knees (**E**, red arrow), abnormal epiphyseal ulna (**F**, red arrow), thoracic scoliosis (**G**, red arrow) and hip anomalies with coxa valga and insufficient acetabular coverage (**H**, red arrow).

Figure 2: Brain MRI studies of *SLC35B2* patients. (**A-C**) Patient 1 (from family A) at 9 months of age: axial T2-weighted (**A-B**) and T1-weighted (**C**) images revealing a supra and infratentorial myelin defect (white arrows).

(**D-F**) Patient 1 (from family A) at 4 years of age: axial T2-weighted (**D-E**) and sagittal T1 (**F**) indicating severe hypomyelination with progressive white matter loss (arrow heads) and thin corpus callosum (asterisk).

(**G-I**) Patient 2 (from family B) at 2.5 months of age: axial T2-weighted (**G-H**) showing absence of myelination (black arrow heads) on posterior limb internal capsules (**G**) and cerebellar peduncles (**H**), and spine MRI revealing early scoliosis as main sign at onset (**I**).

(**J-L**) Patient 2 (from family B) at 36 months of age showing no progression of central myelination and thin corpus callosum (**L**).

(**M-O**) Patient 2 (from family B) at 8 years of age showing severe hypomyelination with mild white matter volume loss.

Figure 3: Identified *SLC35B2* variants and patient family trees. A) Localization of the *SLC35B2* variants relative to the *SLC35B2* gene organization (Striped rectangles indicate the 5'- and 3'- UTRs). **B**) Localization of the *SLC35B2* variants relative to the SLC35B2 protein organization and their consequences on protein structure and sequence (Striped rectangle indicates the C-terminal generated from the frameshift variant). **C**) Patient family trees showing the segregation of the variants with the disease.

Figure 4: *SLC35B2* variant consequences on mRNA level and protein expression. **A**) *SLC35B2* mRNA expression in both control and patient fibroblasts analyzed by RT-PCR. The levels of *SLC35B2* transcript were normalized to those of *GAPDH* and reported as a fold of change in patient cells compared to control cells. Experiments were performed in triplicate. **B, C**) Characterization of wild-type (Wt) and mutant SLC35B2 proteins. HEK293F cells were transfected with plasmids encoding c-Myc tagged wild-type SLC35B2 protein or c-Myc tagged mutant SLC35B2 proteins. **B**) HEK293F lysates were analyzed by western blotting using c-Myc antibody and anti-actin as a loading control (left panel). Scanning density of the bands obtained was used to calculate c-Myc tagged SLC35B2 protein expression levels normalized to those of actin (right panel; AU = arbitrary units). **C**) HEK293F cells were stained with anti-Myc antibody (red), anti-GM130 antibody (green) and nuclei were counterstained with DAPI (blue). Scale bar = 10 µm. The images are representative of three independent experiments. Data are expressed as mean ± SD and significance was determined by two-tailed *t*-test. n.s. = non-significant, **p*-value ≤ 0.05; ***p*-value ≤ 0.01.

Figure 5: CS sulfation pattern in patient and control fibroblasts and Bikunin profile in patient and control sera. A) Sulfation analysis of CS extracted from patient (n=2) and control (n=5) fibroblast culture medium, cultured in basal conditions or with the addition of β-D-xyloside and analyzed by reverse-phase HPLC after digestion with chondroitinase ABC and ACII. ΔDi-0S = non sulfated disaccharide, ΔDi-4S + ΔDi-6S = monosulfated disaccharide. Data are expressed as mean ± SD and significance was determined by two-tailed t-test. ***p*-value ≤ 0.01. **B**) Classical western blot applied to controls (C1 to C4) and patient (Pt) sera, differentiated the core bikunin (Bkn) protein (~24 kDa) and the heterogeneous Bkn-CS form (30-37 kDa). **C**) Schematic representation of hexasaccharide-linked Bkn form (Bkn-Hex) generated after chondroitinase ABC digestion. **D**) 2-DE patterns of control and patients' Bkn-Hex (left panel). The black arrow indicates the loss of negative charges consistent with hyposulfation. Quantification of Bkn sulfation expressed as the % of sulfated and non-sulfated Bkn forms.

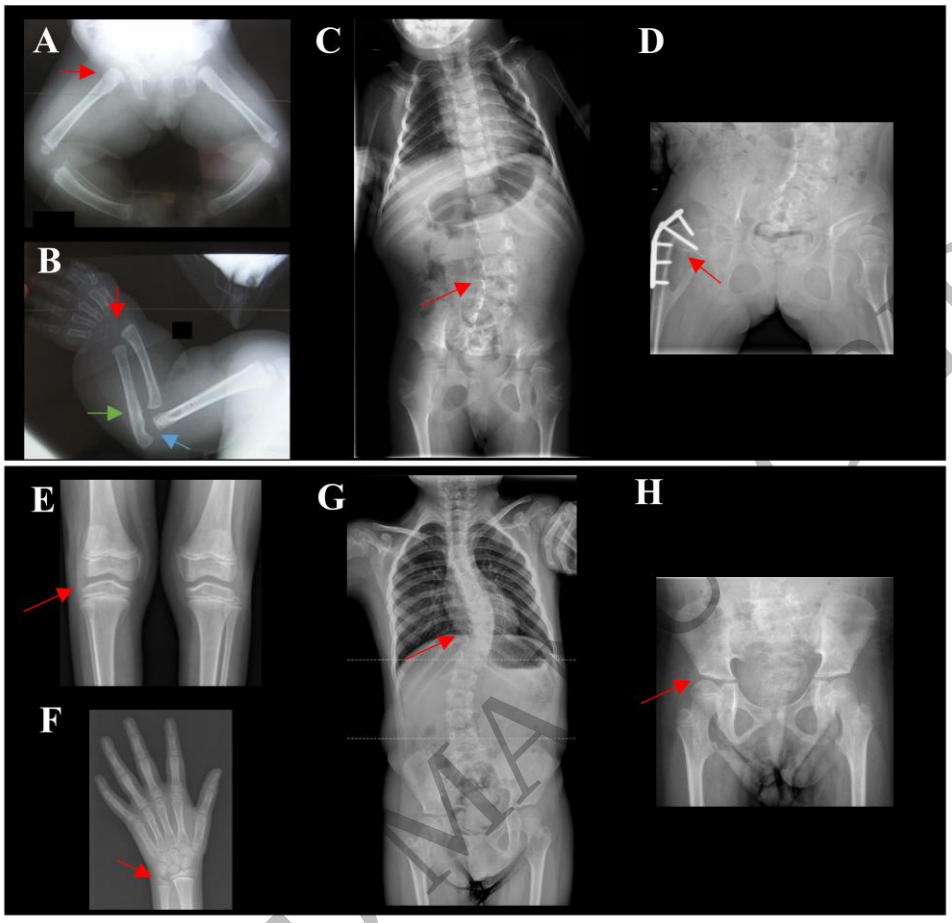

Figure 1
134x128 mm (5.3 x DPI)

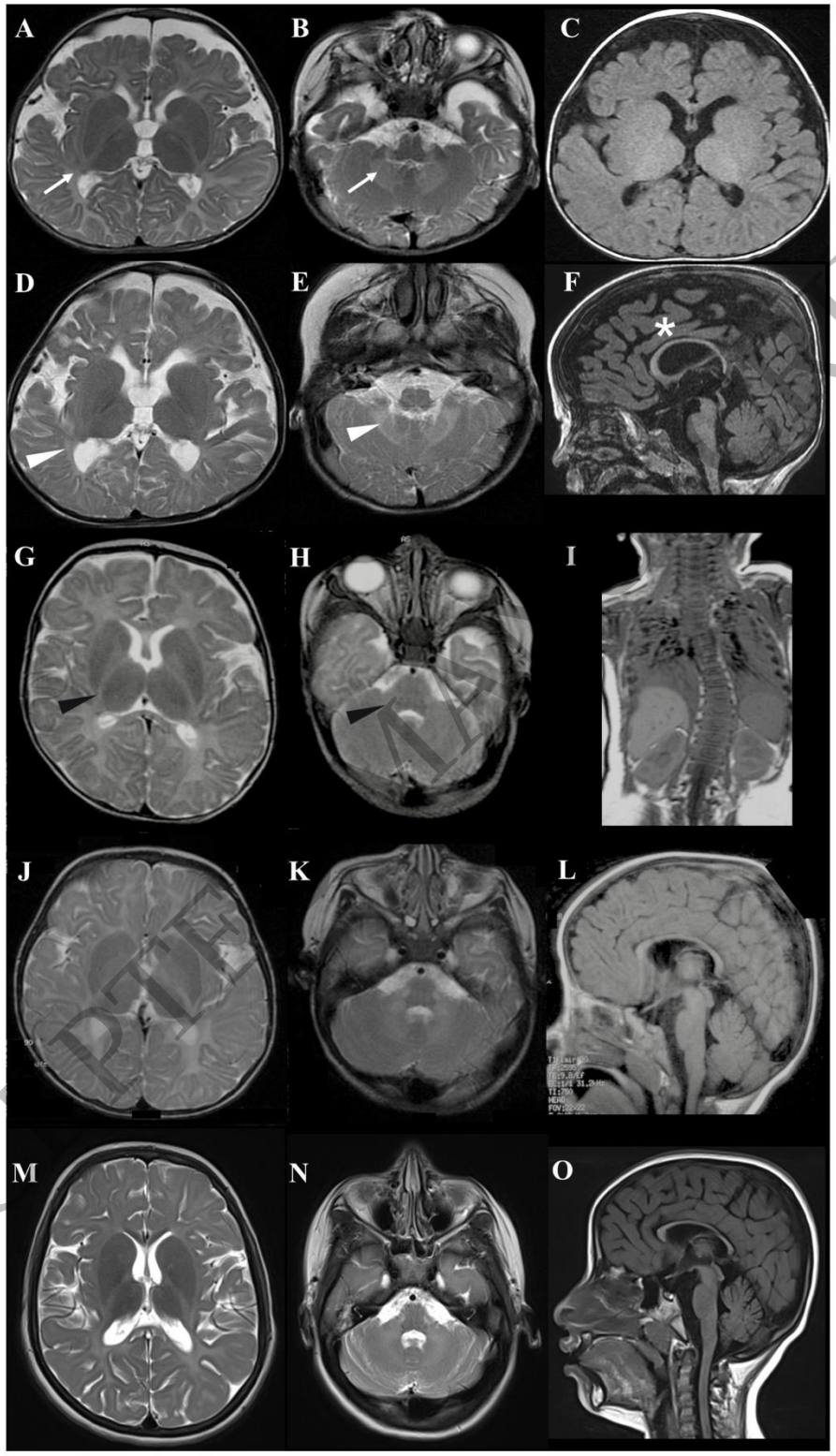

Figure 2
127x216 mm (5.3 x DPI)

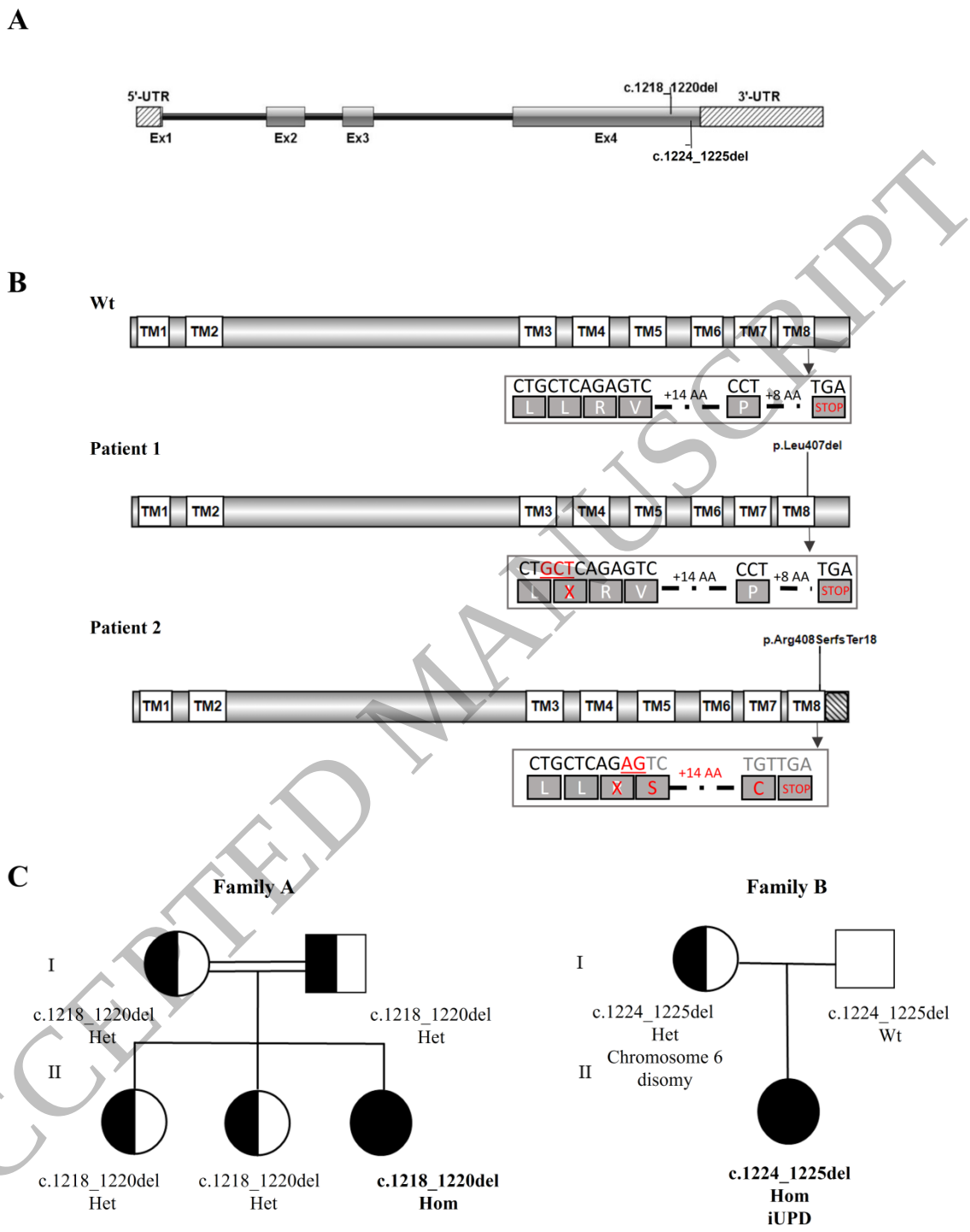

Figure 3
165x226 mm (5.3 x DPI)

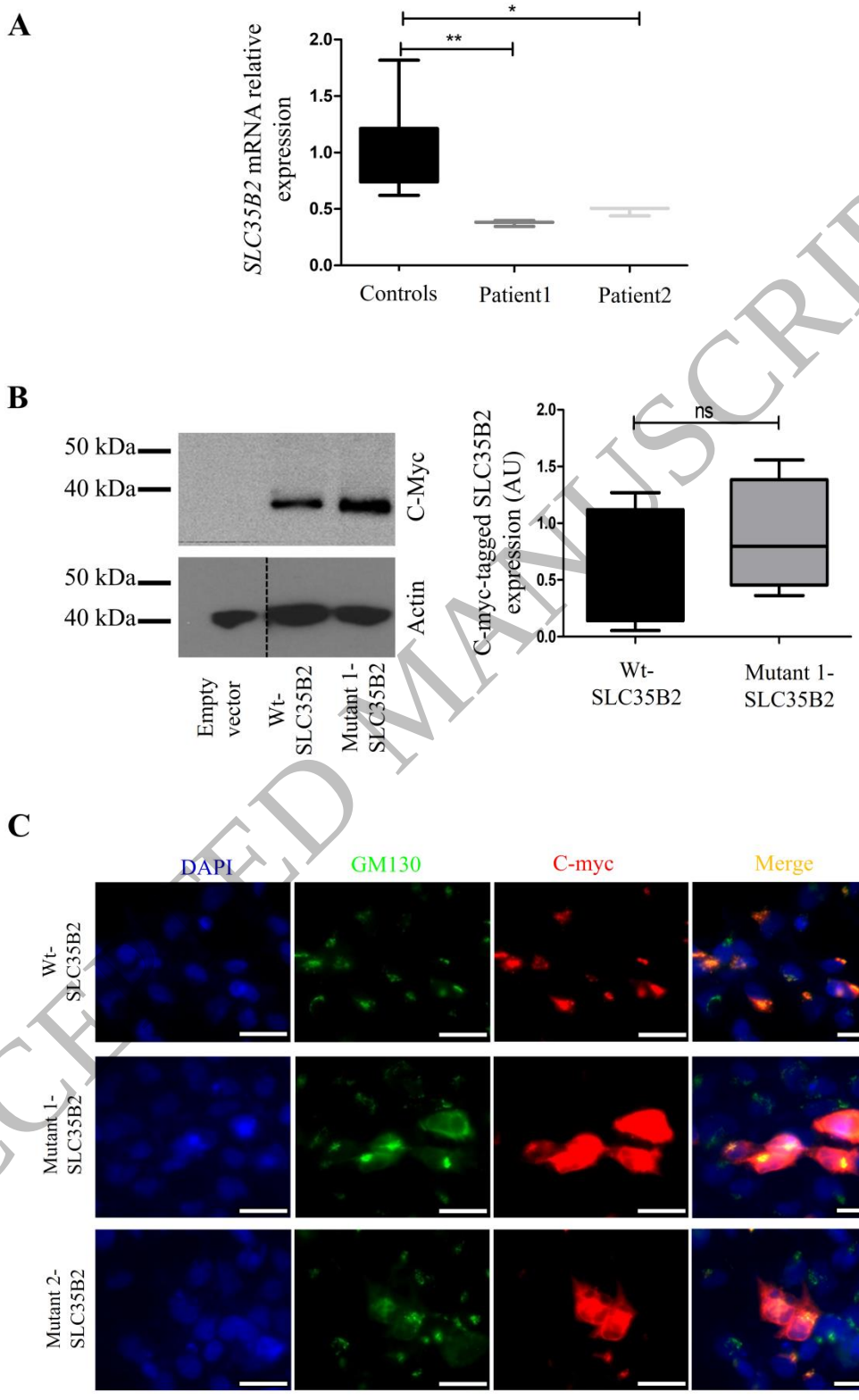

Figure 4
151x229 mm (5.3 x DPI)

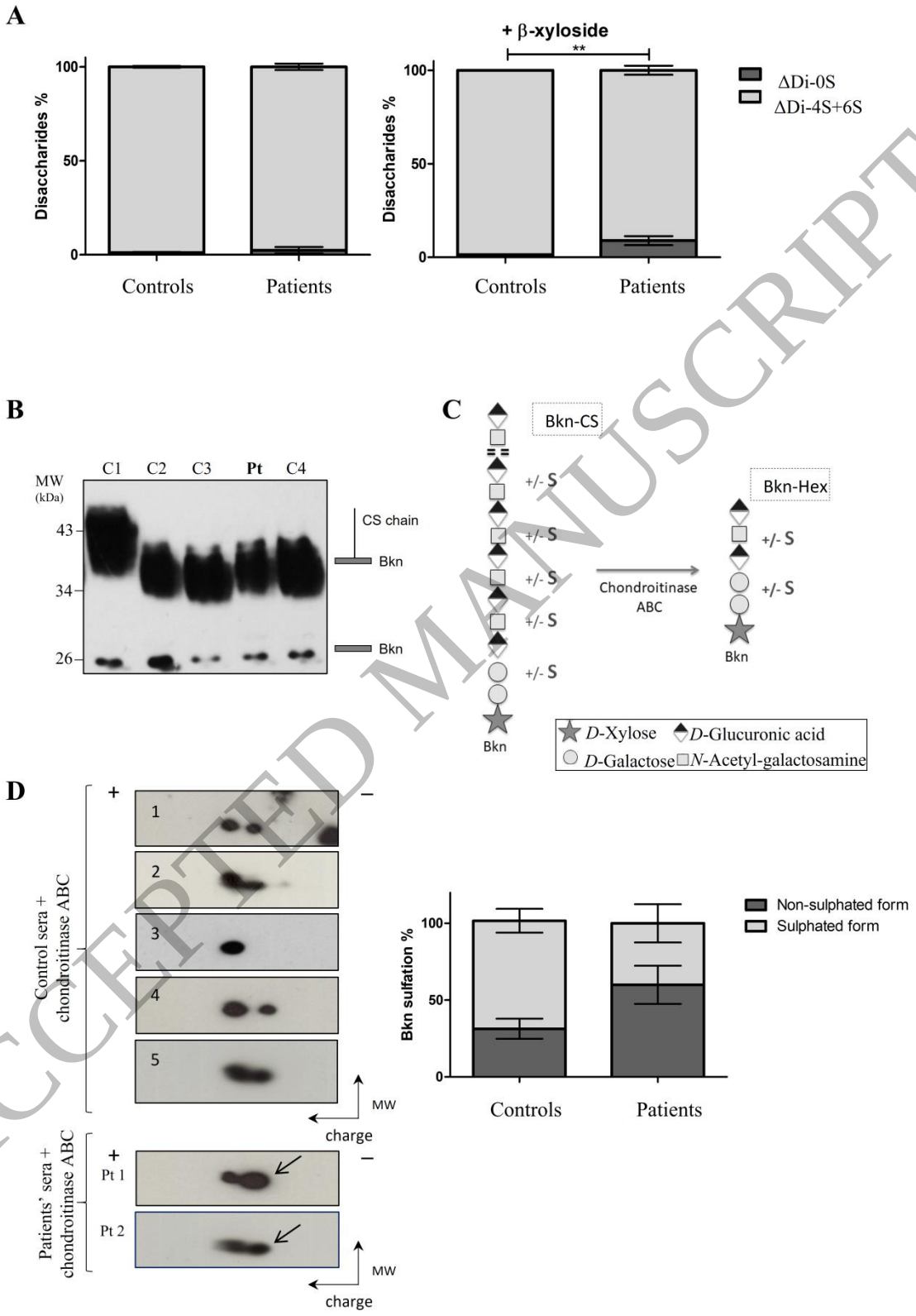

Figure 5
158x229 mm (5.3 x DPI)